Flexible chirp-free probe pulse amplification for kHz fs-ps rotational coherent anti-Stokes Raman scattering

K. Arafat Rahman,[1] Erik L. Braun,[1] Mikhail N. Slipchenko,[1,2] Sukesh Roy,[2] and Terrence R. Meyer[1,*]

[1] *Purdue University, School of Mechanical Engineering, West Lafayette, Indiana 47907, USA*
[2] *Spectral Energies, LLC, 4065 Executive Dr., Beavercreek, Ohio 45430, USA*
**Corresponding author: trmeyer@purdue.edu*

Received XX Month XXXX; revised XX Month, XXXX; accepted XX Month XXXX; posted XX Month XXXX (Doc. ID XXXXX); published XX Month XXXX

The sensitivity of high-repetition-rate hybrid fs/ps rotational coherent anti-Stokes Raman scattering (RCARS) is strongly influenced by the energy available for the ps probe pulse. In this work, a high-energy ps probe pulse that is time-synchronized with the fs pump/Stokes pulse is achieved by using a diode-pumped Nd:YAG amplifier seeded at 1064.4 nm by the output of a fs optical parametric amplifier. Nearly transform-limited, 10 ps pulses with up to 800 μJ/pulse and bandwidth of 1.9 cm^{-1} were generated at the second harmonic 532.2 nm and used for kHz-rate fs/ps RCARS thermometry up to 2400 K with accuracies of 1-2%. We furthermore demonstrate amplification of variable pulsewidths for flexible single-mode (chirp-free) RCARS signal generation.

http://dx.doi.org/10.1364/OL.99.099999

Coherent anti-Stokes Raman scattering (CARS) has been a powerful nonlinear spectroscopic technique for gas-phase species and temperature measurement due to its high spatio-temporal resolution and ability to probe harsh reacting environments [1]. The advent of commercially available kHz-repetition-rate amplified femtosecond (fs) lasers introduced the capability of extending measurements to kHz rates. Initial gas phase fs-CARS thermometry was demonstrated in the time domain [2] and required long duration scanning of a mechanical delay stage. Single-shot chirped probe fs CARS was later developed to map the time domain molecular response to the frequency domain and allowed for thermometry up to 5 kHz [3, 4], albeit with limited ability to isolate chemical species and increased complexity in modeling the nonlinear parameter space associated with the highly chirped probe pulse [5]. For species identification, reduced modeling complexity, and less sensitivity to laser characteristics, an alternative is to utilize a narrowed ps probe pulse to resolve the single-shot CARS spectrum [6, 7]. In this hybrid fs/ps CARS, initial Raman coherences are typically introduced by fs-preparation pulses, namely pump and Stokes, followed by a frequency-narrowed, time-delayed ps-probe pulse that allows for multiplexed detection of the Raman active modes.

The main drawback of hybrid fs/ps CARS comes with generating the narrowband ps pulse. Two general approaches for generating or shaping of the ps probe include: (i) phase-locking separate fs and ps laser systems (two-laser solution), and (ii) generating a narrowband ps pulse derived from the broadband fs pulse (single-laser solution). The former has been employed to demonstrate 20 Hz CARS at a point [8], in a line (1-D) [9], and in a plane (2-D) [10]. This approach has been expanded to 1 kHz 2-D rotational CARS (RCARS) up to 700 K by Miller *et al.* [11]. However, the high cost and experimental complexities of two externally synchronized laser systems obfuscate the path to widespread use.

For the single-laser solution, spectral filtering and nonlinear bandwidth compression have been employed to generate a ps probe from the fs laser source, with a trade-off between spectral characteristics and energy per pulse. The first works on hybrid fs/ps CARS spectral detection [6] and thermometry [12] used a 4-*f* pulse shaper to generate a spectrally narrow, transform-limited probe pulse with variable spectral bandwidth. Follow-on works also utilized an optical filter [13], etalon [14], or volume Bragg grating (VBG) [15] to achieve a similar result, but all led to significant reduction in the probe pulse energy (~10 μJ/pulse) and residual sideband signatures in the spectral and temporal profiles that required care in the experimental and modeling procedures [13, 14]. Alternatively, a second harmonic bandwidth compressor (SHBC) [16] has been used to produce a narrowband (~3.5 cm^{-1}) ps probe pulse by combining two fs pulses with linear chirp in opposite directions in a sum-frequency generation (SFG) crystal with up to 30% conversion efficiency. The ~1.1 mJ/pulse ps probe enabled fs/ps RCARS temperature measurement sensitivity up to 2400 K [17, 18]. However, introduction of imperfect phase conjugation due to instantaneous changes in spatial overlap, difficulty in achieving opposite linear chirp between two pulses, and interferences in the SFG crystal could result in spectral wings and blue shifted satellite pulses [19]. This necessitates careful filtering of the ps probe to avoid non-physical features in the CARS spectra that require

modeling of the laser pulse characteristics or limits probing at certain probe delays. This can be potentially circumvented by combining an SHBC and 4-*f* pulse filter, but this approach has only been shown for RCARS measurements up to 1000 K and using a probe energy of 5 μJ [19].

In this letter, we demonstrate spectral filtering of the output of a fs optical parametric amplifier (OPA) followed by diode-pumped Nd:YAG amplification to generate inherently time-synchronized, spectrally tailored, spectrally pure, transform-limited, high-energy ps probe pulses. This approach is demonstrated for kHz-rate hybrid fs/ps RCARS thermometry with few model corrections in an H_2/Air Hencken burner up to 2400 K. Recently, a similar approach using an Yb:YAG crystal-fiber amplified probe was used to achieve pulse energies of 100 μJ for fs/ps VCARS thermometry up to 3000 K [20]. The current work aims for even higher pulse energies to enable fs/ps RCARS thermometry from ambient to flame temperatures and/or potential extension to 1-D measurements.

The primary laser source was a regeneratively amplified Ti:sapphire laser (Solstice Ace; Spectra-Physics, Inc.) that outputs 100 fs, 7 mJ, 800 nm pulses with a nearly transform-limited bandwidth of ~180 cm^{-1} at 1 kHz, as shown in Fig. 1a. The 800 nm output was split into 3 mJ/pulse and 4 mJ/pulse beam paths, and a portion of the 3 mJ/pulse beam was used for the pump/Stokes beam in the two-beam RCARS setup. The 4 mJ/pulse portion pumped an optical parametric amplifier (TOPAS Prime; Light Conversion, Inc.) to generate the idler at 2128.8 nm, which was subsequently frequency doubled in a BBO crystal to produce 60 μJ/pulse at 1064.4 nm. This beam was then routed to a custom narrowband spectral amplifier (NSA), as shown in Fig. 1b. The NSA consisted of commercially available VBGs (OptiGRATE Corp.), which gives the spectral selectivity of the system, and two diode-pumped Nd:YAG amplifier modules to amplify the selected spectral portion of the beam. The output linewidth of the VBG is inversely proportional to the grating thickness and depends on the refractive index modulation.

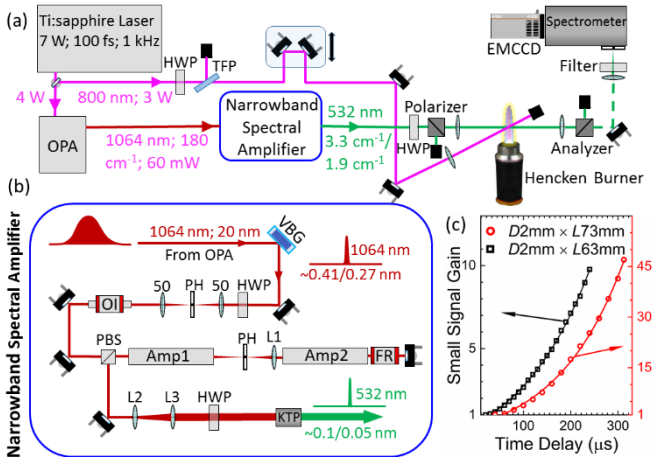

Fig. 1. Experimental set-up. (a) Two-beam RCARS setup. (b) Layout of the narrowband spectral amplifier; VBG: volume Bragg grating, HWP: half wave plate, PH: pinhole, OI: optical isolator, PBS: polarizing beamsplitting cube, TFP: thin film polarizer, FR: Faraday rotator. (c) Small-signal-gain of the diode-pumped Nd:YAG amplifier modules; D: Diameter, L: Length, Solid line: Single exponential fit.

Two different VBGs encoded for ~1064 nm were used with spectral selectivity of 0.41 nm (VBG-I) and 0.27 nm (VBG-II) (measured by MOGLabs, LLC), which correspond to bandwidths of 3.6 cm^{-1} and 2.4 cm^{-1} and output energies of ~0.33 μJ/pulse and ~0.13 μJ/pulse, respectively. The bandwidth of the VBGs were chosen such that two similar irradiance ps probe pulses could be generated at different spectral bandwidths. The spectral filtering of the original fs pulse output from the OPA produces a ps pulse by virtue of the time-bandwidth product (TBP), which is inherently time-synchronized with the mJ-level 800 nm fs pulses used for the pump/Stokes CARS excitation. The spectrally narrowed low energy ps pulses were passed through a spatial filter and optical isolator before being amplified in the diode-pumped Nd:YAG modules. The spatial filter, present before the double-pass amplification stage, facilitates removal of spatial irregularities in the beam profile originating from the OPA and the VBG and is a necessary condition to avoid small-scale self-focusing in the Nd:YAG rods (discussed below) [21].

The small-signal gains (SSG) of the two diode-pumped Nd:YAG modules were measured with a narrowband ns pulsed source near 1064.4 nm and are shown in Fig. 1c. The first amplifier module, Amp1 in Fig. 1b (RBAT24-1P; Northrop Grumman Corp.), has a maximum SSG of 48 with 1 kW of supplied electrical power and a pump duration of 312.5 μs at a repetition rate of 1 kHz. The second amplifier, Amp2 in Fig. 1b (RBA20-1C; Northrop Grumman Corp.) was pumped with a total supplied pump power of 0.8 kW and a 240 μs pump duration at 1 kHz for a maximum SSG of ~10. The diode module drivers were triggered by the fs laser source, and the SSG was measured with respect to this delay. Water cooling was provided for homogenous heat removal from the Nd:YAG rods, and the coolant temperature was optimized and kept constant for maximum gain in each module.

Throughout the experiment, the electrical energy input into the amplifier stages was kept constant while the time delay was varied to change the gain. At the maximum pump level, the focal length of the thermally induced lens in the Amp1 laser rod was ~50 mm, and a pinhole was placed at the focal plane (see Fig. 1b). The focal length of the thermally induced lens in Amp2 was ~300 mm. Lens L1 was used such that the combination of L1 and the thermally induced lens in Amp2 recollimated the beam and completed the relay optics. This arrangement prevented the build-up of ASE and compensated for the thermally induced curvature in the propagating beam wavefront. A 45° Faraday rotator was placed before the 0° mirror to compensate for thermally induced birefringence. The system was designed keeping the gain of Amp2 fixed at its maximum while only varying the gain in Amp1.

The double-pass output energy as a function of input energy for both VBGs is shown in Fig. 2a. The optical isolator and HWP were used to vary the input energy, and the highest output energy was ~650 μJ/pulse and ~1.3 mJ/pulse at 1064.4 nm for VGB-I and VBG-II, respectively. Incorporating losses in the double-pass system, and linear operation in the small-signal regime, the effective SSG was calculated to be ~5 and ~12.5 in Amp1 for the VBG-I and II respectively and ~10 in Amp2 for both cases, which is consistent with the measured values for the corresponding time delay in Fig. 1c. At the maximum output energy, the pulse energy has a standard deviation of ~2.3% of the mean for the system, measured with photodiode sampling for 5 minutes. The measured values for the first 40 seconds are shown in Fig. 2b. The inset in Fig. 2b shows the stability of the spectrally tailored OPA seed source.

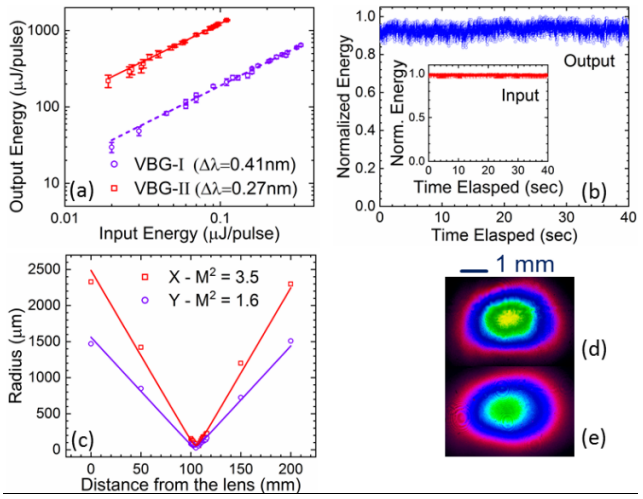

Fig. 2. Amplifier output characteristics at 1064.4 nm. (a) Input vs. output energy for both VBGs; Error bars: ±σ, Solid lines: linear fit. (b) Pulse-to-pulse stability of input and amplified output. (c) Beam quality, M^2. (d) Near-field beam profile. (e) Far-field beam profile.

The quality of the beam, M^2, was measured after L3 as the amplified ps pulse transmitted through a 100-mm focal length lens, and a series of time-averaged beam profiles were acquired along the optical axis for D4σ beam diameter measurements (see Fig. 2c). The M^2 values in x and y were 3.5 and 1.6, respectively. Near- and far-field beam profiles are shown in Figs. 2d and e, respectively. The inferior M^2 in the x-direction was determined to originate from the VBG operating with the broadband OPA output beam and not from any nonlinearities, since the shape of the output beam was found to be independent of the amplified beam intensity.

After two-pass, two-stage amplification, the 1064.4 nm beam was frequency doubled in a 6 mm long KTP crystal (Type II) with a conversion efficiency of ~63% at a fluence of 2 mJ/cm^2. As such, output beam energies of ~400 μJ/pulse (VBG-I) and ~800 μJ/pulse (VBG-II) at 532.2 nm were available to be used in the RCARS experiment. The ~400 μJ/pulse beam had a FWHM bandwidth of 3.3 cm^{-1}, measured after deconvolution with a separately measured 1.7 cm^{-1} spectrograph line-spread function (see Fig. 3a). The time-domain pulse shape was measured by pump-probe intensity cross correlation of the non-resonant signal in argon with the 100 fs pump/Stokes beam and found to be 5.25 ps at FWHM (see Fig. 3b). This yielded a TBP within ~1.1 of the

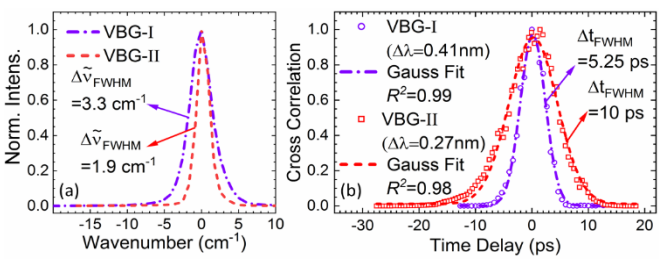

Fig. 3. Frequency and time-domain characteristics of amplified beam after frequency doubling. (a) Measured spectrum of 532.2 nm beam; $\Delta\tilde{\nu}$: bandwidth. (b) Time-domain cross-correlation of the same.

transform limit, and both time and frequency domain pulses showed excellent Gaussian profiles, free from any side-band structure or spectral wings. This eliminates the necessity for pre-processing the ps probe before interaction with pump/Stokes beams and greatly simplifies the RCARS modeling. Similar measurements were performed for the ~800 μJ/pulse 532.2 nm beam (VBG-II). The measured linewidth and time-domain cross-correlation, shown in Fig. 3, had a FWHM bandwidth of ~1.9 cm^{-1} and pulsewidth of ~10 ps.

Self-focusing and self-modulation of short pulses in an active medium due to the electronic Kerr-effect can severely restrict the overall amplification and output beam quality of the amplified pulse [21], and it is a limiting factor for higher gain or shorter pulsewidths. A fraction of the output beam was monitored in a beam profiler to assess potential whole beam self-focusing (WBSF) while increasing the gain in Amp1 for fixed input energy. As the beam traversed the laser rod, the beam power was sufficiently high to induce WBSF during the second pass through Amp1. The length of the Nd:YAG rod was too short for catastrophic collapse of the whole beam at the maximum output of the system, although the gain medium acted as a nonlinear lens. At the maximum output energy of ~1.3 mJ/pulse (VBG-II), the gain medium in the return pass for Amp1 had equivalent focal length of ~450 mm, which is close to the theoretically calculated value of ~430 mm [22]. Moreover, at this combination of short length and ps-duration, frequency broadening due to intensity dependence of the index of refraction is "too slow" to catch up and can be neglected [23]. The overall effect of this nonlinearity can be viewed as an introduction of curvature in the wave-front. Hence, Lenses L2 and L3 (Fig. 1b) were used after the PBS to recollimate and expand the slightly converging beam for frequency doubling. Systems at these conditions are more susceptible to small-scale self-focusing (SSSF), and a good measure of this effect is the so-called *B*-integral [22]. At the maximum output of 1.3 mJ/pulse for the 10-ps duration pulse, the calculated value of *B*-integral was ~1.5, which is lower than the proposed threshold value of 2 for buildup of SSSF [24]. Increasing the gain in Amp1 could yield more energy in the output pulse while staying in the small-signal regime, but above 1.8 mJ/pulse "hot spots" were observed in the amplifying beam, and further increasing the gain could result in SSSF and catastrophic damage to the laser rod. At this point, the calculated *B*-integral was ~2.1. As such, it was safe to restrict the operation up to ~1.3 mJ/pulse to avoid damage in Amp1 and the PBS upstream, where the output beam gets rejected.

Although significant gain narrowing was evident for both VBGs, it was more dominant for VBG-II (from 2.4 cm^{-1} input to 1.9 cm^{-1}) due to much higher gain. This could be a potential mechanism for controlling the linewidth of the output ps-pulse, thus eliminating the need for the VBG before the amplifier modules.

The two-beam RCARS scheme used here was reported in Ref. [25]. The current design ensures jitter-free timing between the pump/Stokes and probe pulses, and a simple delay stage in the pump/Stokes beam path was used to adjust the relative delay of the probe pulse. The pump/Stokes energy was ~100 μJ/pulse or less to avoid self-phase modulation. Two f = 300 mm lenses were used to focus the pump/Stokes and probe beams with a crossing angle of ~30°. The spatial resolution in the direction of probe beam propagation was measured to be 90 μm, which was an order of magnitude better than a similar BOXCARS arrangement [17]. Temperature measurements were carried out in a H_2/Air Hencken burner flame, which produces a nearly adiabatic flame for a wide

range of equivalence ratios (Φ). As the CARS signal co-propagates with the probe, a polarization gating technique was employed to separate the signal beam from the probe beam. To eliminate the residual probe signal that bleeds through the polarization gating, which is comparable to the high-*J* RCARS peaks at flame temperatures, a combination VBG notch filter (OptiGrate; BNF-532-OD3) with 0.3 nm bandwidth at 532 nm and a bandpass filter (Semrock FF01-515/30) were used. However, such filtering was not necessary to access low-*J* transitions at lower temperatures due to the higher signal-to-noise ratio (SNR) achieved by virtue of the N^2 dependency of the CARS signal and sufficient pump/Stokes spectral envelope. The RCARS signal was then dispersed by a 500 mm, 1200 g/mm spectrograph (PI-Acton, 1.7 cm^{-1} measured resolution) onto a back-illuminated EMCCD (Andor).

Processed experimental spectra were fit for temperature using a simple phenomenological N_2-RCARS model. The details of the modeling are laid out previously [26] and will not be presented here. The electric field of the probe pulse was included in the time-domain CARS model as a Gaussian shape with measured spectral and temporal characteristics, and the spectral response of the pump/Stokes pulses was imparted on the convolution of the probe and molecular response via multiplication of the modeled molecular response with an experimentally obtained non-resonant signal in argon [14], measured with the same filters used to acquire the RCARS spectra. The nearly transform-limited Gaussian ps probe optimized the parameter space for the modeling and provided an excellent match with theoretical and single-shot experimental spectra up to ~2400 K (see Fig. 4). Temperature accuracies, estimated as $|(T_{mean}-T_{eq})|/T_{eq}$, are within 2% and are comparable to prior fs/ps VCARS [12] and RCARS [17] data. The precision (1σ of single-shot histograms in Fig. 4) of 2.7% is similar to prior work at ~1900 K. The suboptimal precision of 4.8% at ~2400 K does not necessarily indicate a need for higher probe pulse energy, as the peak SNR is in excess of 20, but rather is readily improved through the use of shorter (spectrally broader) pump/Stokes pulses or spectral focusing [27] to increase the SNR of the high-*J* states.

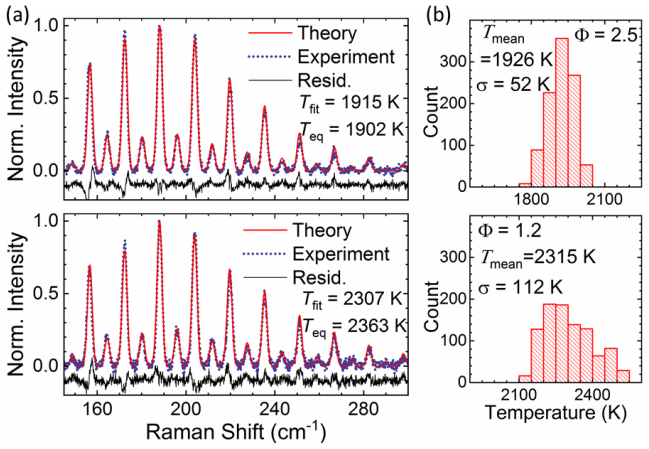

Fig. 4. (a) Example single-shot spectra and the corresponding best-fit simulations at Φ = 2.5 and 1.2, and (b) 1000 single-shot temperature histograms. Probe pulses: 1.9 cm^{-1} bandwidth, 10-ps pulsewidth, and 19.5 ps probe delay. T_{eq}: Adiabatic equilibrium flame temperature.

In summary, we have demonstrated generation of single-mode, high-energy ps-probe pulses from initial fs radiation for kHz-rate hybrid fs/ps RCARS, providing versatility in both spectral resolution selectivity and energy throughput. Transform-limited pulses with 800 μJ/pulse and 1.9 cm^{-1} bandwidth were then utilized for two-beam RCARS thermometry in an H_2/air Hencken burner flame up to 2400 K. Excellent spatial, spectral, and temporal beam quality allowed for fitting the theoretical spectra with a simple Gaussian model for the probe pulse. From the current data on small signal gain, this versatile amplification system has the capability to produce even higher energies by using narrower probe pulses (e.g., 3 mJ/pulse at 532.2 nm with ~0.5 cm^{-1} bandwidth) potentially for measurements at higher repetition rates or kHz-rate 1-D RCARS.

Disclosures. MNS: Spectral Energies, LLC (E); SR: Spectral Energies, LLC (I,E); TRM: Spectral Energies, LLC (C).

References

1. S. Roy, J. R. Gord, and A. K. Patnaik, Prog. Energy Combust. Sci. **36**, 280-306 (2010).
2. R. P. Lucht, S. Roy, T. R. Meyer, and J. R. Gord, Appl. Phys. Lett. **89**, 251112 (2006).
3. S. Roy, W. D. Kulatilaka, D. R. Richardson, R. P. Lucht, and J. R. Gord, Opt. Lett. **34**, 3857-3859 (2009).
4. C. N. Dennis, A. Satija, and R. P. Lucht, J. Raman Spectrosc. **47**, 177-188 (2016).
5. D. R. Richardson, H. U. Stauffer, S. Roy, and J. R. Gord, Appl. Opt. **56**, E37-E49 (2017).
6. B. D. Prince, A. Chakraborty, B. M. Prince, and H. U. Stauffer, J. Chem. Phys. **125**, 044502 (2006).
7. D. Pestov, R. K. Murawski, G. O. Ariunbold, X. Wang, M. Zhi, A. V. Sokolov, V. A. Sautenkov, Y. V. Rostovtsev, A. Dogariu, and Y. Huang, science **316**, 265-268 (2007).
8. A. Bohlin and C. J. Kliewer, Appl. Phys. Lett. **104**, 031107 (2014).
9. A. Bohlin, M. Mann, B. D. Patterson, A. Dreizler, and C. J. Kliewer, Proc. Combust. Inst. **35**, 3723-3730 (2015).
10. M. N. Slipchenko, B. D. Prince, S. C. Ducatman, and H. U. Stauffer, J. Phys. Chem. A **113**, 135-140 (2008).
11. J. D. Miller, M. N. Slipchenko, J. G. Mance, S. Roy, and J. R. Gord, Opt. Express **24**, 24971-24979 (2016).
12. J. D. Miller, M. N. Slipchenko, T. R. Meyer, H. U. Stauffer, and J. R. Gord, Opt. Lett. **35**, 2430-2432 (2010).
13. J. D. Miller, M. N. Slipchenko, and T. R. Meyer, Opt. Express **19**, 13326-13333 (2011).
14. S. P. Kearney, D. J. Scoglietti, and C. J. Kliewer, Opt. Express **21**, 12327-12339 (2013).
15. M. Scherman, M. Nafa, T. Schmid, A. Godard, A. Bresson, B. Attal-Tretout, and P. Joubert, Opt. Lett. **41**, 488-491 (2016).
16. F. Raoult, A. Boscheron, D. Husson, C. Sauteret, A. Modena, V. Malka, F. Dorchies, and A. Migus, Opt. Lett. **23**, 1117-1119 (1998).
17. S. P. Kearney and D. J. Scoglietti, Opt. Lett. **38**, 833-835 (2013).
18. S. P. Kearney, Combust. Flame **162**, 1748-1758 (2015).
19. T. L. Courtney, N. T. Mecker, B. D. Patterson, M. Linne, and C. J. Kliewer, Appl. Phys. Lett. **114**, 101107 (2019).
20. R. Santagata, M. Scherman, M. Toubeix, M. Nafa, B. Tretout, and A. Bresson, Opt. Express **27**, 32924-32937 (2019).
21. S. V. Chekalin and V. P. Kandidov, Phys.-Uspekhi **56**, 123 (2013).
22. W. Koechner, *Solid-state laser engineering* (Springer, 2013), Vol. 1.
23. J. Soures, S. Kumpan, and J. Hoose, Appl. Opt. **13**, 2081-2094 (1974).
24. J. Hunt, K. Manes, and P. Renard, Appl. Opt. **32**, 5973-5982 (1993).
25. M. N. Slipchenko, B. D. Prince, S. C. Ducatman, and H. U. Stauffer, J. Phys. Chem. A **113**, 135-140 (2009).
26. H. U. Stauffer, J. D. Miller, M. N. Slipchenko, T. R. Meyer, B. D. Prince, S. Roy, and J. R. Gord, J. Chem. Phys. **140**, 024316 (2014).
27. S. P. Kearney, Appl. Opt. **53**, 6579-6585 (2014).

Full references (to aid the editor and reviewers):

1. S. Roy, J. R. Gord, and A. K. Patnaik, "Recent advances in coherent anti-Stokes Raman scattering spectroscopy: Fundamental developments and applications in reacting flows," Prog. Energy Combust. Sci. **36**, 280-306 (2010).
2. R. P. Lucht, S. Roy, T. R. Meyer, and J. R. Gord, "Femtosecond coherent anti-Stokes Raman scattering measurement of gas temperatures from frequency-spread dephasing of the Raman coherence," Appl. Phys. Lett. **89**, 251112 (2006).
3. S. Roy, W. D. Kulatilaka, D. R. Richardson, R. P. Lucht, and J. R. Gord, "Gas-phase single-shot thermometry at 1 kHz using fs-CARS spectroscopy," Opt. Lett. **34**, 3857-3859 (2009).
4. C. N. Dennis, A. Satija, and R. P. Lucht, "High dynamic range thermometry at 5 kHz in hydrogen–air diffusion flame using chirped-probe-pulse femtosecond coherent anti-stokes Raman scattering," J. Raman Spectrosc. **47**, 177-188 (2016).
5. D. R. Richardson, H. U. Stauffer, S. Roy, and J. R. Gord, "Comparison of chirped-probe-pulse and hybrid femtosecond/picosecond coherent anti-Stokes Raman scattering for combustion thermometry," Appl. Opt. **56**, E37-E49 (2017).
6. B. D. Prince, A. Chakraborty, B. M. Prince, and H. U. Stauffer, "Development of simultaneous frequency-and time-resolved coherent anti-Stokes Raman scattering for ultrafast detection of molecular Raman spectra," J. Chem. Phys. **125**, 044502 (2006).
7. D. Pestov, R. K. Murawski, G. O. Ariunbold, X. Wang, M. Zhi, A. V. Sokolov, V. A. Sautenkov, Y. V. Rostovtsev, A. Dogariu, and Y. Huang, "Optimizing the laser-pulse configuration for coherent Raman spectroscopy," science **316**, 265-268 (2007).
8. A. Bohlin and C. J. Kliewer, "Two-beam ultrabroadband coherent anti-Stokes Raman spectroscopy for high resolution gas-phase multiplex imaging," Appl. Phys. Lett. **104**, 031107 (2014).
9. A. Bohlin, M. Mann, B. D. Patterson, A. Dreizler, and C. J. Kliewer, "Development of two-beam femtosecond/picosecond one-dimensional rotational coherent anti-Stokes Raman spectroscopy: time-resolved probing of flame wall interactions," Proc. Combust. Inst. **35**, 3723-3730 (2015).
10. M. N. Slipchenko, B. D. Prince, S. C. Ducatman, and H. U. Stauffer, "Development of a simultaneously frequency-and time-resolved Raman-induced Kerr effect probe," J. Phys. Chem. A **113**, 135-140 (2008).
11. J. D. Miller, M. N. Slipchenko, J. G. Mance, S. Roy, and J. R. Gord, "1-kHz two-dimensional coherent anti-Stokes Raman scattering (2D-CARS) for gas-phase thermometry," Opt. Express **24**, 24971-24979 (2016).
12. J. D. Miller, M. N. Slipchenko, T. R. Meyer, H. U. Stauffer, and J. R. Gord, "Hybrid femtosecond/picosecond coherent anti-Stokes Raman scattering for high-speed gas-phase thermometry," Opt. Lett. **35**, 2430-2432 (2010).
13. J. D. Miller, M. N. Slipchenko, and T. R. Meyer, "Probe-pulse optimization for nonresonant suppression in hybrid fs/ps coherent anti-Stokes Raman scattering at high temperature," Opt. Express **19**, 13326-13333 (2011).
14. S. P. Kearney, D. J. Scoglietti, and C. J. Kliewer, "Hybrid femtosecond/picosecond rotational coherent anti-Stokes Raman scattering temperature and concentration measurements using two different picosecond-duration probes," Opt. Express **21**, 12327-12339 (2013).
15. M. Scherman, M. Nafa, T. Schmid, A. Godard, A. Bresson, B. Attal-Tretout, and P. Joubert, "Rovibrational hybrid fs/ps CARS using a volume Bragg grating for N_2 thermometry," Opt. Lett. **41**, 488-491 (2016).
16. F. Raoult, A. Boscheron, D. Husson, C. Sauteret, A. Modena, V. Malka, F. Dorchies, and A. Migus, "Efficient generation of narrow-bandwidth picosecond pulses by frequency doubling of femtosecond chirped pulses," Opt. Lett. **23**, 1117-1119 (1998).
17. S. P. Kearney and D. J. Scoglietti, "Hybrid femtosecond/picosecond rotational coherent anti-Stokes Raman scattering at flame temperatures using a second-harmonic bandwidth-compressed probe," Opt. Lett. **38**, 833-835 (2013).
18. S. P. Kearney, "Hybrid fs/ps rotational CARS temperature and oxygen measurements in the product gases of canonical flat flames," Combust. Flame **162**, 1748-1758 (2015).
19. T. L. Courtney, N. T. Mecker, B. D. Patterson, M. Linne, and C. J. Kliewer, "Hybrid femtosecond/picosecond pure rotational anti-Stokes Raman spectroscopy of nitrogen at high pressures (1–70 atm) and temperatures (300–1000 K)," Appl. Phys. Lett. **114**, 101107 (2019).
20. R. Santagata, M. Scherman, M. Toubeix, M. Nafa, B. Tretout, and A. Bresson, "Ultrafast background-free ro-vibrational fs/ps-CARS thermometry using an Yb: YAG crystal-fiber amplified probe," Opt. Express **27**, 32924-32937 (2019).
21. S. V. Chekalin and V. P. Kandidov, "From self-focusing light beams to femtosecond laser pulse filamentation," Phys.-Uspekhi **56**, 123 (2013).
22. W. Koechner, *Solid-state laser engineering* (Springer, 2013), Vol. 1.
23. J. Soures, S. Kumpan, and J. Hoose, "High power Nd: glass laser for fusion applications," Appl. Opt. **13**, 2081-2094 (1974).
24. J. Hunt, K. Manes, and P. Renard, "Hot images from obscurations," Appl. Opt. **32**, 5973-5982 (1993).
25. M. N. Slipchenko, B. D. Prince, S. C. Ducatman, and H. U. Stauffer, "Development of a Simultaneously Frequency- and Time-Resolved Raman-Induced Kerr Effect Probe," J. Phys. Chem. A **113**, 135-140 (2009).
26. H. U. Stauffer, J. D. Miller, M. N. Slipchenko, T. R. Meyer, B. D. Prince, S. Roy, and J. R. Gord, "Time-and frequency-dependent model of time-resolved coherent anti-Stokes Raman scattering (CARS) with a picosecond-duration probe pulse," J. Chem. Phys. **140**, 024316 (2014).
27. S. P. Kearney, "Bandwidth optimization of femtosecond pure-rotational coherent anti-Stokes Raman scattering by pump/Stokes spectral focusing," Appl. Opt. **53**, 6579-6585 (2014).